



Interpreting cooling dates and histories from laser ablation in-situ (U-Th-Sm)/He thermochronometry

Christoph Glotzbach¹, Todd A. Ehlers^{2,1}

5

¹ Department of Geosciences, University of Tuebingen, Tuebingen, 72076, Germany

² School of Geographical and Earth Sciences, University of Glasgow, G12 8QQ, UK

10

Corresponding author: christoph.glotzbach@uni-tuebingen.de

Abstract

15

Recent applications of the in-situ (U-Th-Sm)/He thermochronometry technique demonstrate its potential to address some of the analytical challenges associated with the whole-grain technique. In this study, we adapted state-of-the-art apatite and zircon production-ejection-diffusion models for application to in-situ dating methods, aiming to enhance the applicability of this technique to a broad range of geologic samples and applications. Our modifications to thermal history models include accommodation of the full range of stopping distances for alpha-particles and cylindrical grain geometries. This investigation focuses on several key aspects of in-situ data interpretation: (i) exploring the relationship between in-situ dates and the position of ablation spots across individual grains, (ii) assessing differences and similarities between whole-grain and in-situ dates, (iii) determining optimal strategies and performance for reconstructing cooling histories from in-situ (U-Th-Sm)/He data, and (iv) reporting the effects of radionuclide zoning on (U-Th-Sm)/He thermochronology. Results indicate that the measured in-situ helium distribution is a function of grain size, ablation spot position and size, and cooling history. Together, these analytical and natural factors result in systematic variations in in-situ dates with distance from the grain rim. Therefore, similar to whole-grain analyses, robust interpretation requires determining grain geometry and the distance of the laser spot to the nearest prismatic face. In most cases, resulting in-situ dates are approximately 30% older than corresponding whole-grain dates, except for samples exhibiting negligible diffusional helium loss. Reconstruction of cooling histories using in-situ (U-Th-Sm)/He data can be achieved through single measurements in several grains with varying grain size and/or effective uranium content, or within a single grain with measurements taken at different distances from the

35



40 grain rim. In addition, statistical analysis of a large compilation of measured radionuclide variations in apatite and zircon grains reveals that radionuclide zoning strongly impacts whole-grain analyses, but can be directly measured with the in-situ method. Overall, our results suggest that in-situ measurements for (U-Th-Sm)/He date determination offer a means to extract meaningful cooling signals from samples with poor reproducibility from traditional whole-grain techniques.

45

1.0 Introduction

50 Alpha decay of radiogenic isotopes and related ingrowth of ^4He in crystal grains is the basis of the widely applicable (U-Th-Sm)/He method (e.g. Lippolt et al., 1994, Wolf et al., 1996, Farley, 2002). A wide variety of minerals incorporate trace amounts of naturally occurring alpha-emitting isotopes such as U, Th, and Sm. Among those minerals, apatite and zircon have some favourable properties, making them a common choice for a wide range of applications to problems in tectonics and surface processes (e.g., Farley, 2000, 55 2002; Gallagher et al., 1998; Reiners and Ehlers, 2005; Malusà and Fitzgerald, 2019). Most importantly, apatite and zircon are abundant in many rock types, have a well-defined He diffusion behaviour (e.g., Farley, 2000; Reiners, 2005; Hourigan et al., 2005; Flowers et al., 2009; Guenther et al., 2013), and are sensitive to upper crustal temperatures (e.g., Ehlers, 2005; Reiners and Brandon, 2006). Most applications of apatite and zircon (U-Th-Sm)/He 60 thermochronometry make use of this and invert (U-Th-Sm)/He data to retrieve cooling histories of exhumed rocks (e.g. Wolf et al., 1996). The majority of (U-Th-Sm)/He thermochronometry studies use multiple whole-grain measurements from a single sample, often in combination with other thermochronometric data (e.g. Flowers 2009; Guenther et al., 2017; Falkowski et al., 2023). This is possible because He diffusion in apatite and zircon 65 is controlled by grain size and accumulated radiation damage, both of which vary from grain to grain and thus lead to sample- and thermal history-specific relationships between these parameters. An alternative method to reveal the near-surface thermal history of rocks is the $^4\text{He}/^3\text{He}$ method (Shuster and Farley, 2004), which indirectly measures the He profile by stepwise degassing of He from proton-irradiated apatite grains.

70 Irrespective of the method applied, deriving accurate cooling histories is often difficult because of biases introduced by (i) crystal fragmentation (Brown et al., 2013), (ii) fluid inclusion or inclusion of radionuclide-rich mineral phases (e.g., Farley, 2002; Ehlers and Farley, 2003; Vermeesch et al., 2007; Danišik et al., 2017), (iii) implantation of He from radionuclide-rich phases from outside the grain (Spiegel et al., 2009), and (iii) radionuclide



75 zonation and related variability of diffusion caused by radiation damage (e.g., Hourigan et
al., 2005; Fox et al., 2014, Anderson et al., 2017). Careful selection of euhedral grains free
of visible inclusion can prevent large biases caused by the first two processes. In the case of
detrital studies where the date distribution is the target, excluding grains can introduce bias
in the resulting date distributions. Despite the previous complications, the in-situ (U-Th-
80 Sm)/He method can be applied even though part of a grain is unsuitable and can
theoretically provide less biased results (e.g., Tipathy-Lang et al., 2013). Radionuclide
zoning and the implantation of He are usually not accounted for in common (U-Th-Sm)/He
protocols. Zonation increases the variance in whole grain (U-Th-Sm)/He dates and is likely
the main cause for overdispersed dates (e.g. Horne et al., 2016, 2019).

85 Shortly after the implementation of using defocused infrared lasers for whole grain (U-
Th-Sm)/He analysis (House et al., 2000), the in-situ (U-Th-Sm)/He method was introduced
by Boyce et al. (2006). However, in-situ dating has not become a routine alternative to
whole-grain measurements, despite several studies demonstrating the reliability of dating
large and/or rapidly cooled monazite, zircon, and apatite age standards (e.g. Boyce et al.,
90 2006; Tripathy-Lang et al., 2013; Evans et al., 2015). One potential issue is that more
common small grains with less rapid cooling suffer from partial He loss by diffusion and thus
should result in older (U-Th-Sm)/He ages (e.g. Tipathy-Lang et al., 2013).

In this study, we explore the measurement procedures required to interpret in-situ (U-
Th-Sm)/He dates and retrieve cooling histories from multiple measurements in several
95 grains or from a single grain. To do this, we simulate the He concentration across grains as
a function of grain size/shape, radionuclide zoning and cooling history. These predicted He-
distributions across grains are used to investigate the relationship between the size and
position of in-situ laser ablation spots and the corresponding in-situ (U-Th-Sm)/He dates.
The in-situ determined dates are then compared to predicted whole-grain dates to identify
100 the usability and limitations of each technique. In addition, the effect of radionuclide zoning in
apatite and zircon on whole-grain dates is studied based on a large LA-ICP-MS dataset. We
find that single in-situ (U-Th-Sm)/He measurements from different grains from the same
sample, or multiple measurements within a single grain can be successfully inverted to
retrieve consistently complex cooling histories similar to whole-grain analyses.

105

2.0 Methods

2.1 Modelling approach for He production, ejection and diffusion

110



115 The in-situ (U-Th-Sm)/He method is based on the extraction of He, U, Th and Sm from
a small fraction of the grain using a laser ablation system (e.g. Boyce et al., 2006; Tripathy-
Lang et al., 2013; Evans et al., 2015; Anderson et al., 2017; Pickering et al., 2020). Ablation
pits can have a radius of a few tenths of μm and depths of a few μm (e.g., from an excimer
laser). Importantly, the ratio of He to U, Th and Sm (and therefore the date) varies with the
size and position of the laser ablation measurements and likely differs from corresponding
whole-grain (U-Th-Sm)/He dates. This, however, does not mean that dates are wrong or not
interpretable; instead, they require a refinement of the interpretation steps commonly applied
to (U-Th-Sm)/He data.

120 Whole-grain (U-Th-Sm)/He analyses use a sphere-equivalent radius and assume
spherical isotropic diffusion to estimate whole-grain He production, ejection, and diffusion in
apatite/zircon crystals (e.g. Farley et al., 1996; Meesters and Dunai, 2002). More effort is
required to match grain geometry for the in-situ (U-Th-Sm)/He method since long-alpha
stopping distances (up to several tens of μm) result in a complex geometric relation between
125 the location of radionuclides (U, Th and Sm) and the resulting position of produced He. Most
apatite grains have a prismatic geometry, with typical length/radius ratios of 4-8 (Farley,
2000), and thus can be approximated with a finite cylinder model (Meesters and Dunai,
2002). Farley et al. (2011) provide a method to transform measured element concentrations
from cylindrical grains into an equivalent spherical-geometry, ready to be used as input in
130 the commonly used modelling software HeFTy (e.g. Danišik et al., 2017). Conversely to this
approach, here we used the available spherical model implemented in HeFTy (Ketcham,
2005) and modified it to handle an infinite cylinder geometry. The latter should be a good
approximation for in-situ measurements outside the tips/caps of the analyzed grains where
alpha-ejection effects become more significant. The advantage of an infinite cylinder model
135 (compared to a finite cylinder model) is that it can be solved in 1D and thus runs as fast as
the spherical model, a prerequisite for applying efficient inverse thermal history modelling.
We adjusted the available He production, ejection, and diffusion models implemented in
HeFTy (Ketcham, 2005; Flowers et al., 2009; Guenther et al., 2013) to handle an infinite
cylinder geometry. More specifically, we implemented our changes to the existing C++ code
140 (kindly provided by R. Ketcham) that simulates He diffusion following the RDAAM (apatite,
Flowers et al., 2009) and ZRDAAM (zircon, Guenther et al., 2013) diffusion and annealing
models. The modified version of RDAAM and ZRDAAM code is available from the Zenodo
repository (<https://zenodo.org/records/10531763>).

145

2.2 Geometric considerations for He production, ejection and diffusion



The amount of He produced vs. ejected and diffused out of the grain depends on the concentration and distribution of parent isotopes and the grain morphology. These effects differ in spherical and cylindrical grains, especially if grains are zoned. The latter has been implemented in diffusion models for spheres (e.g., in HeFTy), which we also explore here for an infinite cylinder geometry. For simplicity, we assume that radionuclide zoning is symmetric around the c-axis for cylindrical grains (Fig. 1). Radionuclide zoning and grain size (especially the distance to the grain rim) control the amount of He along the radius (r-axis), without diffusion. The He distribution along the r-axis is calculated by modelling the intersecting lines of all alpha-ejection spheres (ranging from ~6 to ~40 μm) and internal cylinders with a radius defined by the grain size and grid spacing. The intersection line can consist of two closed curves, a continuous line, or, if the cylinder and the sphere are tangential to each other at one point, the line forms an 'eight' geometry, also known as Viviani's curve (Fig. 1A).

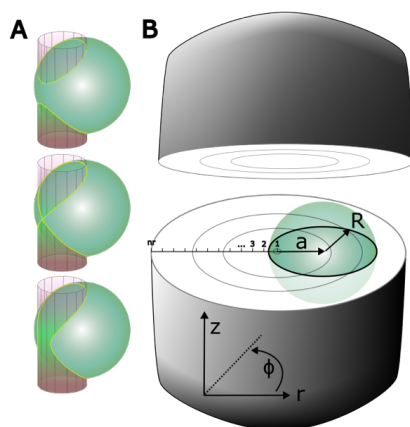


Fig. 1: Geometric relationship between alpha-ejection spheres (green) and intersecting inner grain coaxial cylindrical surface representing variable radionuclide concentrations in a cylindrical grain (light grey lines). A) The length of a line defining the intersection between the cylinder with a sphere depends on the size of each object and their positions. B) Assumed cylindrical grain with radionuclide zoning parallel to the z-axis is intersected by an alpha-ejection sphere with radius R and distance from the centre of a . The modelled He profile is discretized from the centre of the grain to the rim with nodes from $i=1 \dots nr$.

170

The procedure for calculating the amount of He in an infinite cylinder without diffusion along the r-axis is:



175 1. The grain is discretized by a number of cylinders (r, Φ, z), and the circular shape of the cylinders in r, Φ -plane is transformed in x, y -coordinates:

$$x_{r,\phi} = r \cos(\Phi) \quad (1)$$

$$y_{r,\phi} = r \sin(\Phi) \quad (2)$$

180 2. The z -coordinates of the intersection line between the cylinder and the alpha-ejection sphere (the yellow line in Fig. 1A) are calculated with:

$$z_{r,\phi,R,a} = R^2 - (x_{r,\phi} - a)^2 - y_{r,\phi}^2 \quad (3)$$

185 where R is the radius of the alpha-ejection sphere, and a is the distance between the centre of the cylinder and the alpha-ejection sphere, and Φ and r are the same as in Fig. 1B.

190 3. The length of the intersection line is calculated with the Pythagorean theorem:

$$l_{r,R,a} = 2 \sum_{i=1}^{n\Phi-1} \sqrt{(x_{r,R,a}(\Phi_i) - x_{r,R,a}(\Phi_{i+1}))^2 + (y_{r,R,a}(\Phi_i) - y_{r,R,a}(\Phi_{i+1}))^2 + (z_{r,R,a}(\Phi_i) - z_{r,R,a}(\Phi_{i+1}))^2} \quad (4)$$

where Φ has been discretized from 0 to 2π into $i=1 \dots n\Phi$.

195

4. Next, the length is normalized to unity:

$$\check{l}_{r,R,a} = \frac{l_{r,R,a}}{\sum_{i=1}^{na} l_{r,R}(a_i)} \quad (5)$$

200

where a has been discretized from $r=0$ to the rim into $i=1 \dots na$.

5. Finally, we derived the radionuclide-specific concentration ($C_{l,a}$) for isotopes (l) and points (a) along the r -axis with:

205
$$C_{l,a} = \sum_{j=1}^{nR} F_{l,j} \sum_{i=1}^{nr} \check{l}_{r,a}(R_j) C(r_i) \quad (6)$$



where F_{ij} is the fractional contribution of an isotope-specific stopping distance and C is the radionuclide concentration depending on r .

210 The resulting He distribution is very similar to a spherical grain, but with an overall
higher concentration (for similar radii) since we assume an infinite length of the cylinder (Fig.
2). Incorporating He diffusion and alpha-stopping distances leads to smooth (uniform
radionuclides) or complex (zoned grains) He profiles (Fig. 2,5).

215

2.3 Calculation of He diffusion

Assuming a spherical grain geometry provides a good estimate of whole-grain He
diffusion in apatite crystals (e.g., Farley et al., 1996; Meesters and Dunai, 2002). But, most
220 apatite and zircon grains have a prismatic shape. Here we solved the production and
diffusion equation for an infinite cylinder (Farley, 2000). The 3D diffusion equation in a
cylinder is:

$$\frac{1}{r} \frac{\partial}{\partial r} \left(rK \frac{\partial v}{\partial r} \right) + \frac{1}{r^2} \frac{\partial}{\partial \phi} \left(K \frac{\partial v}{\partial \phi} \right) + \frac{\partial}{\partial z} \left(K \frac{\partial v}{\partial z} \right) + A_0 = \frac{\partial v}{\partial t} \quad (7)$$

225

where v is the He quantity, K is the diffusivity, t is time, A_0 is the volumetric He
production, and r , z and ϕ are the radial, vertical and azimuth positions (e.g., Fig. 1B).
Assuming an infinite length of the cylinder and that He does not vary with z and ϕ , the
equation (Eq. 7) simplifies to:

230

$$\frac{1}{r} \frac{\partial}{\partial r} \left(rK \frac{\partial v}{\partial r} \right) + A_0 = \frac{\partial v}{\partial t} \quad (8)$$

Using the product rule, we get:

$$235 \quad \frac{K}{r} \frac{\partial v}{\partial r} + K \frac{\partial^2 v}{\partial r^2} + A_0 = \frac{\partial v}{\partial t} \quad (9)$$

We solved Equation 9 with an implicit Euler finite difference method with the following
assumptions: (i) grain symmetry (including geometry and radionuclide distribution) around
the z -axis, (ii) zero-flux Neumann boundary condition in the centre of the grain (Eq. 10), and
240 (iii) infinite diffusion at the grain boundary (Eq. 11):



$$\frac{\partial v}{\partial r} = 0 \quad \text{for } r=0 \quad (10)$$

$$v = 0 \quad \text{for } r=\text{rim} \quad (11)$$

245 Reformulating equation (Eq. 9 and 10) with the implicit Euler method yields:

$$\frac{v_i^{t+1} - v_i^t}{\Delta t} = \frac{K}{r} \frac{v_{i-1}^{t+1} - v_{i+1}^{t+1}}{\Delta r} + K \frac{v_{i-1}^{t+1} - 2v_i^{t+1} + v_{i+1}^{t+1}}{\Delta r^2} + A_0 \quad \text{for } r>0 \ \& \ r<\text{rim} \quad (12)$$

$$\frac{v_i^{t+1} - v_i^t}{\Delta t} = K \frac{v_{i-1}^{t+1} - v_{i+1}^{t+1}}{\Delta r} + A_0 \quad \text{for } r=0 \quad (13)$$

250 Since $i=-1$ is not defined, but similar to $i=+1$, it is common to instead use the second derivative and Eq. 13 changes to:

$$\frac{v_i^{t+1} - v_i^t}{\Delta t} = K \frac{2v_{i+1}^{t+1} - 2v_i^{t+1}}{\Delta r^2} + A_0 \quad \text{for } i=0 \quad (14)$$

255 Preparing to solve Equation 14 requires a tridiagonal matrix whereby all unknowns ($t+1$) are brought to the left-hand side:

$$(1 + 2D)v_i^{t+1} - 2Dv_{i+1}^{t+1} = v_i^t + A_0\Delta t \quad \text{for } i=0 \quad (15)$$

$$\left(-\frac{D\Delta r}{r} - D\right)v_{i-1}^{t+1} + (1 + 2D)v_i^{t+1} + \left(\frac{D\Delta r}{r} - D\right)v_{i+1}^{t+1} = v_i^t + A_0\Delta t \quad \text{for } r>0 \ \& \ r<\text{rim} \quad (16)$$

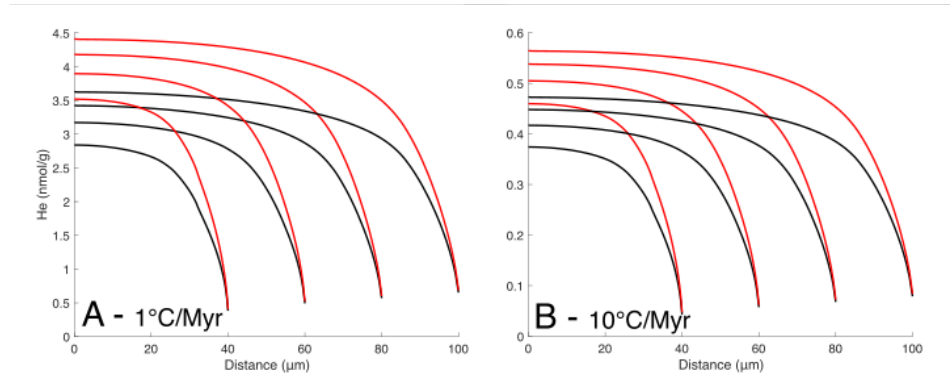
$$260 \quad v_i^{t+1} = 0 \quad \text{for } r=\text{rim} \quad (17)$$

where D is $K\Delta t/\Delta r^2$, and the corresponding tridiagonal matrix needed to solve for diffusion in an infinite cylinder is given by:

$$265 \quad \begin{pmatrix} 1 + 2D & -2D & 0 & 0 & \dots & 0 \\ -\frac{D\Delta r}{r} - D & 1 + 2D & \frac{D\Delta r}{r} - D & 0 & \dots & 0 \\ 0 & -\frac{D\Delta r}{r} - D & 1 + 2D & \frac{D\Delta r}{r} - D & \dots & 0 \\ \vdots & \vdots & \vdots & \vdots & \ddots & \vdots \\ 0 & 0 & 0 & 0 & 0 & 1 \end{pmatrix} \begin{pmatrix} v_{i=0}^{t+1} \\ v_{i=1}^{t+1} \\ v_{i=2}^{t+1} \\ \vdots \\ v_{i=r+1}^{t+1} \end{pmatrix} = \begin{pmatrix} v_{i=0}^t + A_0\Delta t \\ v_{i=1}^t + A_0\Delta t \\ v_{i=2}^t + A_0\Delta t \\ \vdots \\ 0 \end{pmatrix} \quad (18)$$

The resulting He profiles for infinite cylinders have similar shapes as a sphere, but higher He concentrations than a sphere with the same radius (Fig. 2). The difference in concentration between the infinite cylinder and sphere geometry (for constant cooling) is in the range of 15-20% in the centre of the grain, comparable to previous observations (Meesters and Dunai, 2002).

270



275 Fig. 2: Difference between He diffusion profiles in a sphere (black) and infinite cylinder
 (red) with grain radii of 40, 60, 80 and 100 μm . All profiles are based on homogenous U, Th
 and Sm distributions with 10 ppm and constant cooling rates of 1°C/Myr (A) and 10°C/Myr
 (B).

280 A cylindrical model is a good approximation for the He profile in hexagonal apatite
 grains (Meesters and Dunai, 2002), but it is unclear what radius should be used to estimate
 the He profile. To determine the appropriate cylinder radius to approximate diffusion in a
 hexagonal grain, we calculated the 2D (cross-sectional) He distribution of an infinite long
 symmetrical hexagonal grain with circumradius r_c between 30-50 μm and corresponding
 285 infinite cylinders with variable radii. We measured the difference between the mean He
 profile of the hexagonal and cylindrical grains and found that the circle-equivalent radius
 (CER) of a symmetrical hexagonal grain is simply the radius of a circle with a similar area:

$$290 \quad CER_{ap} = \sqrt{\frac{\frac{3\sqrt{3}}{2}r^2}{\pi}} \approx 0.9094r \quad (19)$$

where r is the outer radius (touching all vertices) of a symmetrical hexagon. Equivalent
 to a zircon with a quadratic cross-section, we derived the following:

$$295 \quad CER_{zr} = \sqrt{\frac{2r^2}{\pi}} \approx 0.5642r \quad (20)$$

where r is the outer radius of a quadrate.



300

2.4 Implementation of alpha-stopping distances

During alpha decay, energy is released that leads to long alpha-stopping distances (e.g. Bragg and Kleeman, 1905). The common radiogenic isotopes ^{238}U , ^{235}U , ^{232}Th , and ^{147}Sm release alpha decay energies between 2233 keV (^{147}Sm to ^{143}Nd) and 8784 keV (^{212}Po to ^{208}Pb as part of the decay chain of ^{232}Th). In total, the alpha decay of these radionuclides produces 216 different energies, each occurring with a different probability (Fig. 3). The relation between energy and stopping distance has been measured and calculated and is easily accessible from the SRIM data collection (e.g., Farley et al., 1996; Ketcham et al., 2011). Alpha particles produced from ^{238}U , ^{235}U , and ^{232}Th have stopping distances between 310 ~ 11 and ~ 40 μm in apatite (Fig. 3A-C), and those derived from ^{147}Sm have a single stopping distance of ~ 6 μm . Integration of the stopping distance distribution yields the average stopping distances (Fig. 3A-C), commonly used to approximate He distribution profiles and F_T correction factors for whole-grain analyses (e.g., Ketcham et al., 2011). Note that the reported values using the SRIM 2013 data show only very small differences from those of 315 Ketcham et al. (2011), which is based on SRIM 2008.

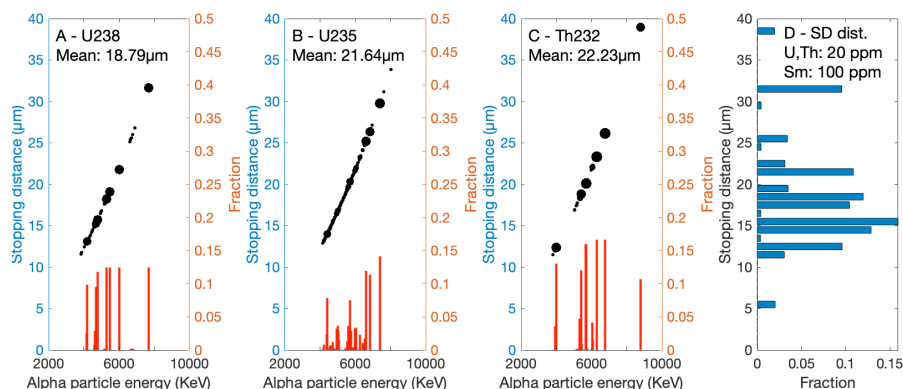


Fig. 3: Alpha particle energy spectra of ^{238}U (A), ^{235}U (B), and ^{232}Th (C) and the corresponding stopping distance spectra and mean stopping distances derived from SRIM2013 data assuming a fluorine apatite with a density of 3.2 g/cm^3 . The stopping distance distribution (SD dist.) of a typical apatite with 20 ppm U and Th, and 100 ppm Sm is shown in (D).

Depending on the relative concentration of radionuclides, each mineral crystal will 325 have a grain-specific alpha-stopping distance distribution (Fig. 3D). The majority of stopping distances in apatite are between 11 and 26 μm , with additional peaks at 6 μm , 32 μm , and



39 μm for a common apatite (Fig. 3D). Stopping distances in zircons are shorter and less variable, ranging from 9 to 32 μm , while the majority are between 10 and 26 μm long (Fig. S1). Due to the long alpha-stopping distances, the in-situ measured He in an infinitely small area within the grain is produced from the surrounding ~ 6 to 39 μm and ~ 9 to 32 μm in apatite and zircon, respectively. Importantly, He originates from the surface of spheres with a radius corresponding to the stopping distance distribution (Fig. 4). This does not have large consequences for grains with a homogenous radionuclide distribution, but He and radionuclide distributions do not follow a 1:1 relation in the case of radionuclide heterogeneity in grains (Fig. 4).

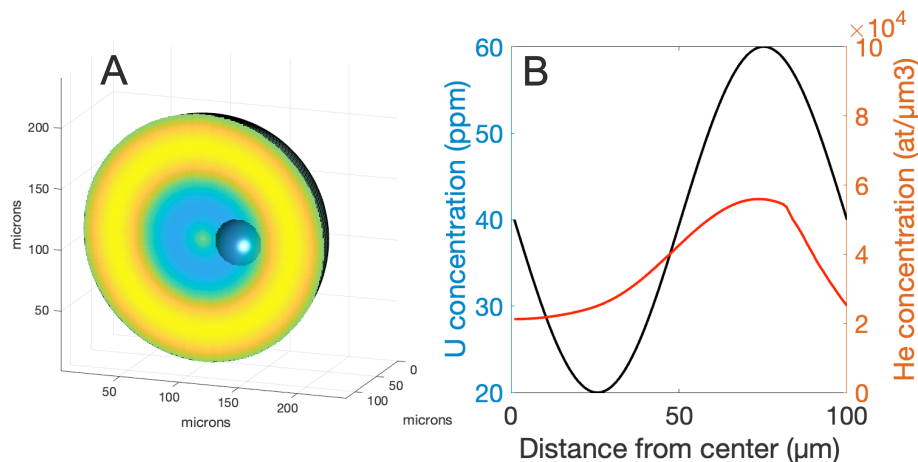


Fig. 4: Relationship between radionuclide zonation and resulting He profiles in a spherical apatite grain. A) Spherical grain with radial U, Th and Sm concentrations between 20 to 60 ppm, respectively. The small half-sphere corresponds to a stopping distance of 20 μm . B) U, Th, Sm and resulting He concentrations from the core to the rim of the grain shown in A.

As a consequence, we adjusted the original RDAAM and ZRDAAM c++ implementation of HeFTy to (i) handle the full spectrum of stopping distances (instead of using an averaged value) of respective radionuclides and (ii) incorporate inner grain radionuclide variations.

We tested our extended implementation against the original implementation for a theoretical spherical apatite grain (Fig. 5). The resulting whole-grain dates are indistinguishable from each other but the He profiles produced are smoother and, in some cases, show distinct differences (Fig. 5). Considering the full spectrum of stopping distances results in an overall lowering of the He concentration when approaching the grain rim for uniform radionuclide distributions (Fig. 5A). The incorporation of longer stopping distances



(up to 39 μm) results in reduced He production at a distance between the longest stopping distance and the mean stopping distance from the grain rim. The opposite effect (higher He concentrations nearer to the grain rim) originates from stopping distances shorter than the mean stopping distance (Fig. 5A). Spherical grains with a grain radius smaller than the longest stopping distance (39 μm) but larger than the mean stopping distance (~ 20 μm) show lower He concentrations since the production in the grain core is zero when the grain radius is smaller than the stopping distance (Fig. 5A). Variations in radionuclides, such as at the boundary between the grain and exterior require consideration of the full spectrum of stopping distances in case of in-situ (U-Th-Sm)/He analyses close to the grain rim (within 39 μm from the grain rim). Similarly, a mean stopping distance approach results in dissimilar He profiles in zoned grains with radionuclide variations compared to considering the full spectrum (Fig. 5B). To give an example, a two times higher radionuclide concentration between half and three-quarters of the radius (measured from the centre) results in the largest differences in the He concentration in the centre of the grain. The latter is usually the target of in-situ (U-Th-Sm)/He analyses. We propose that any in-situ (U-Th-Sm)/He analyses require considering the full spectrum of significantly contributing alpha-stopping distances. Although not investigated here, the $^4\text{He}/^3\text{He}$ method might also benefit from considering this to predict more accurate He profiles (e.g., Shuster and Farley, 2004).

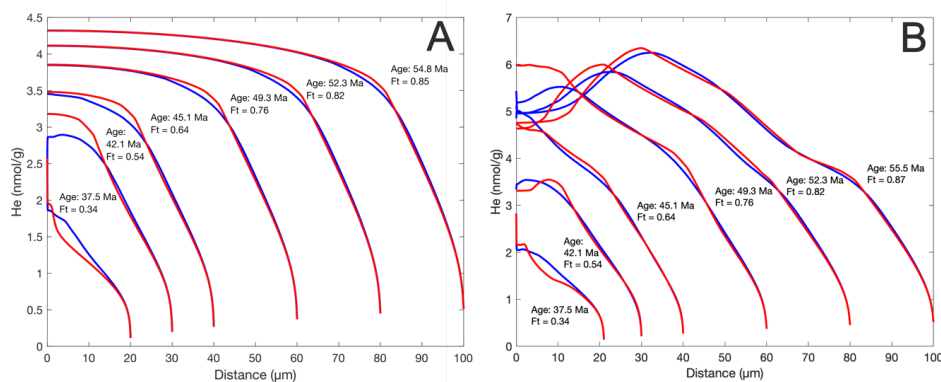


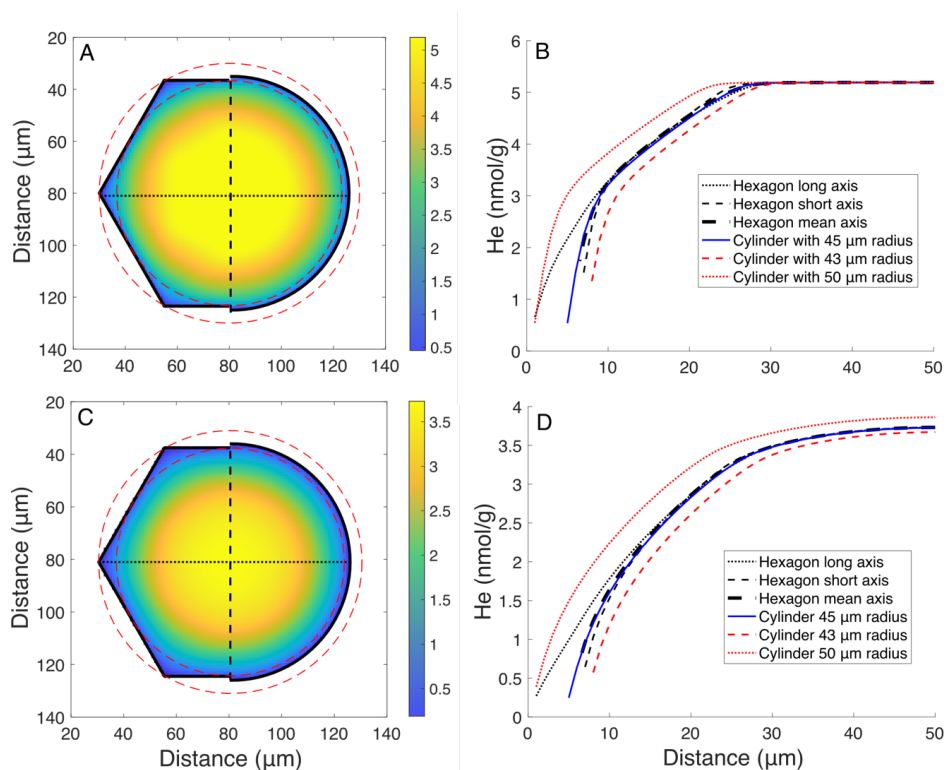
Fig. 5: Apatite He profiles and (U-Th-Sm)/He dates for a cooling rate of $1^\circ\text{C}/\text{Myr}$, variable grain sizes, and mean (red, original implementation) or complete stopping distances (blue, our implementation). A) Uniform U, Th and Sm concentration of 10 ppm. B) Same as in A) but with two times higher radionuclides between the half radius and $\frac{3}{4}$ radius.

2.5 Circle Equivalent Radius (CER)



380

Modelling (U-Th-Sm)/He data is usually accomplished using a transient 1D axial-symmetric parameterization, where different grain morphologies are approximated with a spherical geometry with similar volume-to-surface area ratios. With this approach, a solution is calculated in 1-D (as a function of radius), and then integrated over the volume of the equivalent sphere. It has been shown that this approach is accurate for common grain morphologies within a few percent, whereas an infinite cylinder can have a deviation of up to 7% (e.g. Meesters and Dunai, 2002). Here we explore if such an approach also applies to accurately estimating He profiles within grains. We modelled the He distribution of an infinite symmetrical hexagonal prism with an outer radius of 50 μm (inner radius of 43.3 μm). We compared these results to those calculated with an infinite cylinder (Fig. 6). The CER for such a grain is $\sim 45.5 \mu\text{m}$. The mean He profile of the hexagonal prism after averaging all possible profiles from the centre of the grain to the edge are nearly identical to a cylinder with a radius of 45.5 μm . This result is irrespective of the cooling history (Fig. 6). The He profile deviates substantially at the outermost 5-10 μm between the long and short axis of a hexagon, which should be discarded if it is not exactly known where the short and long axes are relative to the location of measurement.





400 Fig. 6: He concentration in infinite hexagonal prism and cylinder. A) He concentration
map modelled with RDAAM for a symmetrical hexagonal prism with an outer radius of 50 μm
and cylinder with a radius of 45.5 μm , and 10 ppm U, Th and Sm concentrations, and rapid
cooling (100°C/Myr) to surface temperature (10°C) at 60 Ma. B) Corresponding He profiles
for a hexagonal prism and infinite cylinder with different radii. C/D) Similar to A/B but for a
405 constant cooling rate of 1°C/Myr.

3.0 Results

410 3.1 Whole-grain vs. in-situ (U-Th-Sm)/He dates

Whole-grain (U-Th-Sm)/He dates reflect the production, ejection, diffusion, and alpha-
ejection correction for the complete grain. In contrast, in-situ (U-Th-Sm)/He dates, if
measured in the centre of grains, are not affected by alpha ejection, less affected by
diffusion, and do not require an alpha-ejection correction (e.g., Tripathy-Lang et al., 2013).
415 Theoretically, in-situ dates will, in most cases, differ from whole-grain dates from similar
grains. Most in-situ (U-Th-Sm)/He studies applied so far used large crystals with
homogenous radionuclide distributions and/or rapidly cooled samples to enable comparison
to the results to whole-grain measurements (e.g., Boyce et al., 2006; Horne et al., 2016).
420 Making this method applicable to small and/or slowly cooled grains requires understanding
the relationship between the grain size, position and size of the ablation spots, radionuclide
distribution, and resulting (U-Th-Sm)/He dates.

First, we modelled whole-grain and in-situ (U-Th-Sm)/He dates as a function of cooling
rate (1, 10 and 40°C/Myr) for radionuclide concentrations of 10 ppm and a grain radius of
425 100 μm (Fig. 7A-C). Modelled whole-grain dates are 49, 6.5 and 1.9 Ma for cooling rates of
40, 10 and 1°C/Myr, respectively. In-situ (U-Th-Sm)/He dates vary as a function of their
measurement position in the grain. Assuming similar grain parameters and cooling rates, in-
situ dates range between 48-65 Ma (1°C/Myr), 6.3-8.3 Ma (10°C/Myr) and 1.8-2.4 Ma
(40°C/Myr) for a spot diameter of 20 μm and grain radius of 100 μm (Fig. 7A-C). Modelled in-
430 situ dates measured in the centre of grains are older than the whole-grain dates since the
fraction of He lost by diffusion is smallest in the centre of grains and increases towards the
grain boundary, as does He loss by alpha-ejection. Accordingly, in-situ dates become
progressively younger towards the grain rim. A larger laser spot size averages over a larger
area and may incorporate areas affected by He loss. A larger spot size, therefore, leads to



435 younger dates, and a smaller spot size can be expected to produce less variation in dates,
especially when analyzing smaller grains.

Second, we simulated the effect of grain size on whole-grain and in-situ (U-Th-Sm)/He
dates for a cooling rate of 1°C/Myr, radionuclide concentrations of 10 ppm and grain radii of
100, 80, 50 and 40 μm (Fig. 7C-F). Whole-grain dates decrease as a function of grain size
440 from 49 to 39 Ma, while in-situ dates consistently result in older dates. In-situ measurements
with similar spot diameter (e.g., 20 μm) sample larger fractions of areas affected by He loss
and, therefore, in-situ dates become less sensitive to the measurement position in the grain
for smaller grains. In the most extreme case where the spot diameter corresponds to the
grain radius the alpha-ejection corrected in-situ date would match the whole-grain date. In
445 practice, the spot size also depends on the expected He concentration and must be
determined based on the detection limit of He measurable with the instrumental setup and
the maximum depth of laser pits that can be measured accurately.

Third, we studied the in-situ date dependency for cases in which grains have not been
ground and polished to the exact centre of the grain (Fig. 7G,H). In-situ dates become
450 progressively younger towards the grain rim compared to a measurement in the centre of the
grain (Fig. 7G,H). In a large grain (100 μm radius, Fig. 7G), dates are similar within <40 μm
from the central plane of the grain. In-situ dates in smaller grains are more sensitive to the
position of the measurement relative to the grain rim (Fig. 7H).

In summary, uniform cooling yields in-situ (U-Th-Sm)/He dates that are older than
455 whole-grain dates, and dates strongly vary as a function of the measurement position
relative to the grain rim. The results obtained here for apatite also apply to zircons, as has
been revealed by modelling in-situ dates as a function of grain size, and position and size of
the ablation spots with the ZRDAAM approach (Fig. S2). Measuring grain size and
geometry, and the laser spot position relative to the grain rim is essential for correctly
460 interpreting in-situ (U-Th-Sm)/He dates. The grain size and geometry, and location of laser
pits on the grain surface can be easily determined with an optical microscope, whereas
estimating the pit location in the vertical direction is difficult. A rough estimate ($\pm 5 \mu\text{m}$) can
be gained by focusing on the contact between grain and embedding media and measuring
the distance to the exposed grain surface.

465

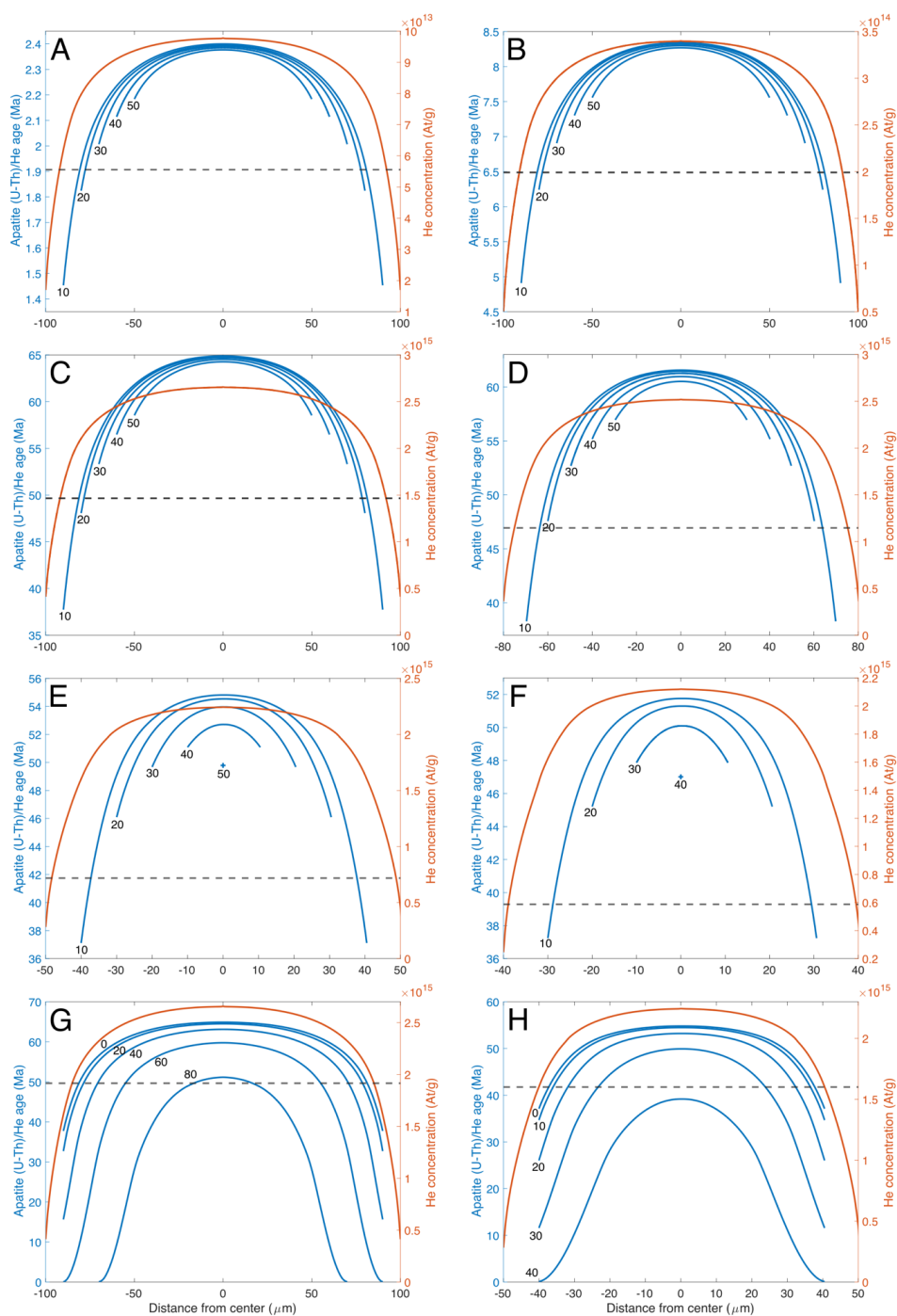


Fig. 7: Predicted in-situ apatite (U-Th-Sm)/He dates (blue lines) and He concentration profile (orange line) for an infinitely long, cylindrical-shaped apatite with homogenous



radiogenic nuclide distribution (U, Th and Sm concentration of 10 ppm). Predicted dates are
470 calculated by integrating the modelled He distribution over an entire ablation pit volume of
variable diameters (black numbers on curves in A-D), which is continuously measured
across the grain. In reality, discrete (rather than continuous) pits would be measured, and
smooth curves such as those shown here would not be possible. A) Model results assuming
a constant cooling rate of 40°C/Myr to a final temperature of 10°C and a grain radius of 100
475 µm. The corresponding whole-grain date for a sphere with a similar sphere-equivalent radius
(radius*1.5) corrected for alpha ejection is 1.9 Ma. Modelled in-situ dates with variable spot
diameters (10, 20, 30, 40 and 50 µm) range from 2.4 Ma in the centre of the grain to 1.45 Ma
half the spot diameter away from the grain rim. B) Model results assuming constant cooling
at 10°C/Myr to 10°C and a grain radius of 100 µm. The corresponding whole-grain date
480 corrected for alpha ejection is 6.5 Ma. Modelled in-situ dates with variable spot diameters
(10-50 µm) range from 8.3 Ma in the centre of the grain to 4.8 Ma half the spot diameter
away from the grain rim. C) Model results assuming constant cooling at 1°C/Myr to 10°C and
a grain radius of 100 µm. The corresponding whole-grain date corrected for alpha ejection is
64.9 Ma in the centre of the grain to 37.7 Ma half the spot diameter away from the grain rim.
485 D,E,F) Same as C) but with a grain radius of 80, 50, and 40 µm. The smaller grain radius
results in younger whole-grain dates (47, 42, and 39 Ma, respectively) and a stronger
relationship between in-situ dates and distance of measurement towards the grain rim. G) In-
situ dates for a grain radius of 100 µm and spot diameter of 10 µm. Dates have been
calculated for the central plane, dividing the cylinder into two symmetrical sides along the
490 crystallographic c-axis (black number 0 - 0 µm in the r-direction of Fig. 1) and at other r-
planes 20, 40, 60, and 80 µm. H) In-situ dates for a grain radius of 50 µm and spot diameter
of 10 µm. Dates have been calculated for the central plane and at other r-planes 10, 20, 30,
40 µm.

495 3.2 Effects of radionuclide zoning

Without efficient methods to quantify inner-grain variations in radionuclides, whole-
grain analyses commonly use an apriori assumption of a uniform radionuclide distribution.
The in-situ (U-Th-Sm)/He dating technique produces spatially resolved (albeit averaged over
500 the ablation pit) measurements of U, Th, and Sm (e.g. Horne et al. 2016, Danišik et al.,
2017). In-situ measurements can provide information about inner-grain radionuclide
variations and potentially lead to a reduction in date variability when taking into account
heterogeneities in the radionuclides.

Here, we have analyzed several hundred LA-ICP-MS measurements done in our lab at
505 the University of Tuebingen, Germany. The depth-resolved radionuclide measurements in



apatite and zircon demonstrate that radionuclide zoning is common (supplement data SD1). Zoning is more common and pronounced in zircons; ~30% of all analyzed zircons have a core-to-rim ratio <0.5 or >2, whereas this fraction is at ~10% for apatites (Fig. S4). Not accounting for radionuclide zoning results in erroneous Ft-correction factors and resulting whole-grain dates (e.g., Hourigan et al. 2005). Here, we use our updated production-ejection-diffusion model to calculate the relationship between whole-grain (U-Th-Sm)/He dates and radionuclide variations (Fig. 8).

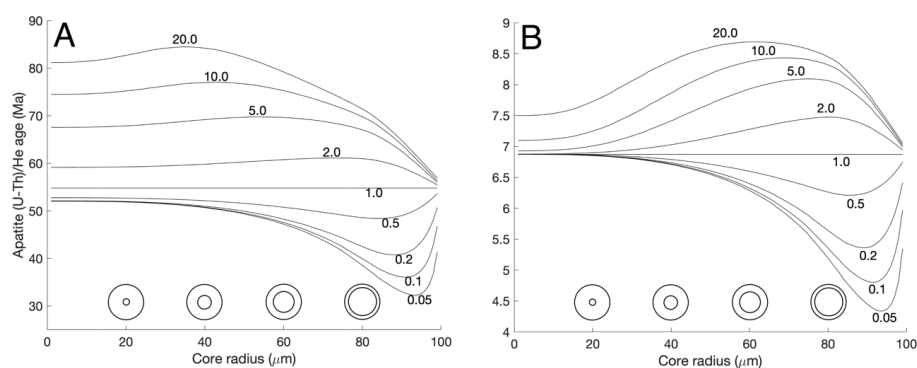


Fig. 8: Whole-grain apatite (U-Th-Sm)/He dates as a function of radionuclide variations (zoning). Isoline labels correspond to the core/rim ratio of radionuclides, assuming a single-step function in the concentration of U, Th, and Sm across the grain, where the x-axis specifies the location of the step in concentration. A) Dates for a cooling rate of 1°C/Myr and volume-averaged U, Th, and Sm concentration of 10 ppm. B) Dates for a cooling rate of 10°C/Myr and volume-averaged U, Th, and Sm concentration of 10 ppm.

Commonly observed core-to-rim ratios between 0.5 and 2 lead to $\pm 10\%$ date deviations (Fig. 8). Since observed radionuclide variations cannot be simplified with a single-step function (Fig. S3), we have scaled measured LA-ICP-MS derived depth variations to a grain radius of 100 μm and calculated whole-grain apatite and zircon (U-Th-Sm)/He dates for a cooling rate of 1 $^{\circ}\text{C}/\text{Myr}$ (Fig. 9). Single-grain dates are mainly a function of the mean eU of individual grains, but depending on the amount of radionuclide zoning, dates deviate from the corresponding date assuming homogenous radionuclide distribution (red line in Fig. 9). The correlation coefficient is 0.95 and 0.77 for all apatites and zircons, respectively, or, in other words, 5% and 23% of the variability in dates is the result of radionuclide zoning. Individual samples usually involve fewer grains with variations in dates caused by radionuclide zoning ranging from 1 to 40% and 19 to 84% for analyzed apatites and zircons (Fig. 9), respectively. In samples with a low variation in eU and strong radionuclide zoning,



the majority of variability is caused by zoning and there is no significant relation with eU. For
535 example, in the analyzed Fish Canyon tuff zircons, 84% of the variations in dates is due to
zoning (Fig. 9B). As mentioned earlier, additional age dispersion can come from crystal
fragmentation, radionuclide-rich inclusions, fluid inclusions and implantation of He from the
exterior (e.g. Brown et al., 2013; Vermeesch et al., 2007; Spiegel et al., 2009; Danišik et al.,
2017). It is, therefore, more likely to have overdispersed whole-grain (U-Th-Sm)/He dates,
540 and perfect relations between dates and eU will be the exception rather than the rule.

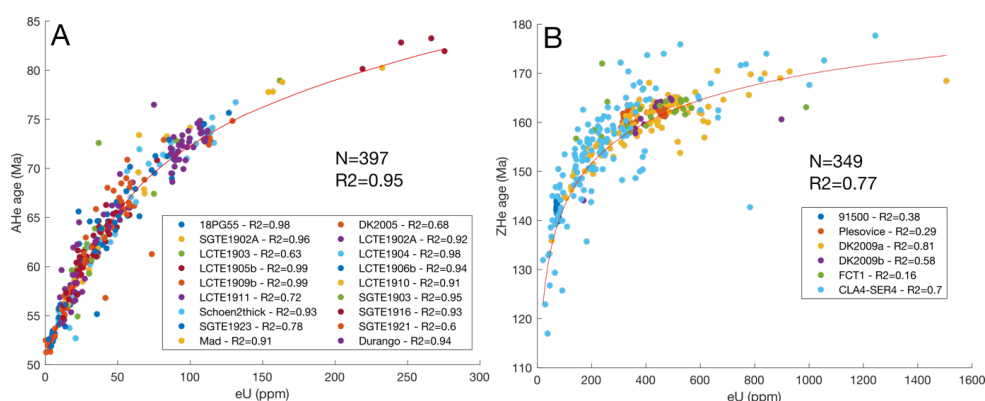


Fig. 9: Simulated apatite (A) and zircon (B) (U-Th-Sm)/He dates for a constant cooling
rate of 1°C/Myr, and measured grain-specific U, Th, and Sm variations (coloured dots).
545 Radionuclide variations were measured in age standards and random samples with an LA-
ICP-MS system and scaled to a common grain size of 100 μm , assuming symmetric zoning
around the c-axis. This was used to model grain-specific whole-grain (U-Th-Sm)/He dates.
The red line represents the relation between dates and homogenous radionuclide
distribution. The correlation coefficient for the whole dataset and individual samples are
550 shown. Note that the $1-R^2$ is the fraction of spread caused by radionuclide zoning.

The observed radionuclide variations and resulting date dispersion in Figure 9 allow for
estimating the minimum sample size required to reach a defined correlation coefficient
between date and eU. We used a Monte Carlo approach to determine the relationship
555 between the correlation coefficient and sample size and found that a minimum of 10 apatite
grains is needed to reach an R^2 of 0.8, and an impractical 23 whole-grain ZHe dates are
theoretically needed to reach a minimum R^2 of 0.5 (see supplement data SD3 for details).

In summary, whole-grain (U-Th-Sm)/He age variations with eU are often biased by
radionuclide zonation. Measuring depth-resolved information on radionuclide variation in
560 apatite and zircon grains allows the identification of zoned grains for exclusion from further
analyses. Since this analytical step is mandatory for the in-situ (U-Th-Sm)/He method,



single-grain data should, in theory, lead to less dispersion in date vs. eU plots and likely also produce more reliable thermal history reconstructions.

565

3.3 Thermal history modelling of in-situ (U-Th-Sm)/He data

The relative distribution of He within an apatite or zircon grain is a function of the distribution of radionuclides, grain morphology, and the cooling history. A suite of whole-grain analyses can be used to reconstruct potential cooling histories under the precondition that analyzed grains have different grain sizes and/or eU (e.g., Ketcham, 2005; Flowers et al., 2009; Gautheron et al., 2009; Guenther et al., 2013). This approach, however, has the risk of including grains with internal variations in radionuclides, and is, therefore, often applied in combination with other thermochronometric systems (e.g., apatite fission track data). The apatite $^4\text{He}/^3\text{He}$ method is a more robust but complex method (Shuster and Farley, 2004), which indirectly measures the He profile by a stepwise degassing of He from proton-irradiated apatite grains.

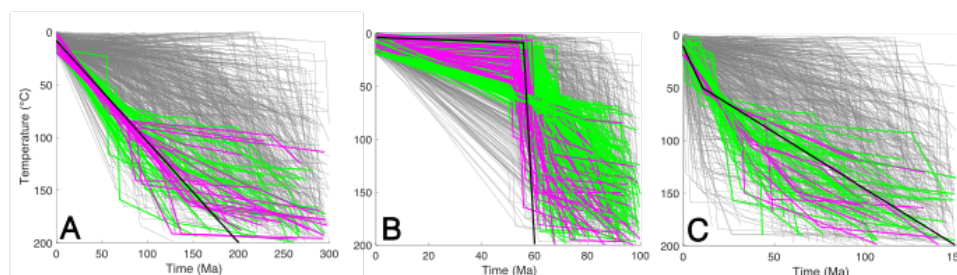
Thermal history modelling with in-situ (U-Th-Sm)/He data could be done by (i) measuring multiple grains that vary in size and/or eU similar to the whole-grain approach, or (ii) reconstructing the He profile with multiple measurements in a single grain comparable to the $^4\text{He}/^3\text{He}$ method (e.g. Danišić et al., 2017). Both approaches are applied in the following to reconstruct common cooling paths from synthetic datasets. A robust methodology requires knowing or estimating (i) grain geometry, (ii) the position of the in-situ measurements within the grain, (iii) the radionuclide distribution within the grain, and (IV) building an appropriate model to account for the previous factors.

In theory, complex grain morphologies could be used for such an approach, but this would require implementing grain-specific 3D models. Thermal history modelling with such 3D models is time-consuming and, therefore, not practical for routine analysis. Similar to whole-grain analyses, it is therefore recommended to make in-situ measurements of grains with simple geometries characterized by straight and/or 2D-3D constant curvatures such as spherical, elliptical, and cylindrical shapes. Preferably, the in-situ measurement can be approximated with a 1D modelling approach similar to whole-grain and $^4\text{He}/^3\text{He}$ analyses, where the sphere-equivalent radius has been shown to be a good approximation (e.g. Meesters and Dunai, 2002; Farley et al., 2010). Unlike whole-grain and $^4\text{He}/^3\text{He}$ analyses, the in-situ method requires modelling the He concentration within the ablated pit volume.

We conducted two different measurement approaches to evaluate the utility of in-situ dating techniques for thermal history reconstruction. First, a set of two spot measurements in the centre of sphere-shaped grains with radii of 80 and 40 μm and similar eU were forward-



600 modelled with three different cooling histories: (1) a constant cooling rate of 1°C/Myr, (2)
rapid cooling of 100°C/Myr at 60 Ma to surface temperature followed by no cooling, and (3) a
step-increase in cooling rate from an initial 1°C/Myr until 10 Ma to 50°C, followed by 4°C/Myr
cooling to surface temperature. After adding 10% uncertainty to the in-situ (U-Th-Sm)/He
dates, several thousand forward models were conducted, and the goodness-of-fit (GOF) of
605 predicted cooling paths was determined. We used the same definition of the GOF and colour
scheme as used in HeFTy (Ketcham, 2005). Good and acceptable model paths retrieve the
input cooling paths in most cases (Fig. 10).

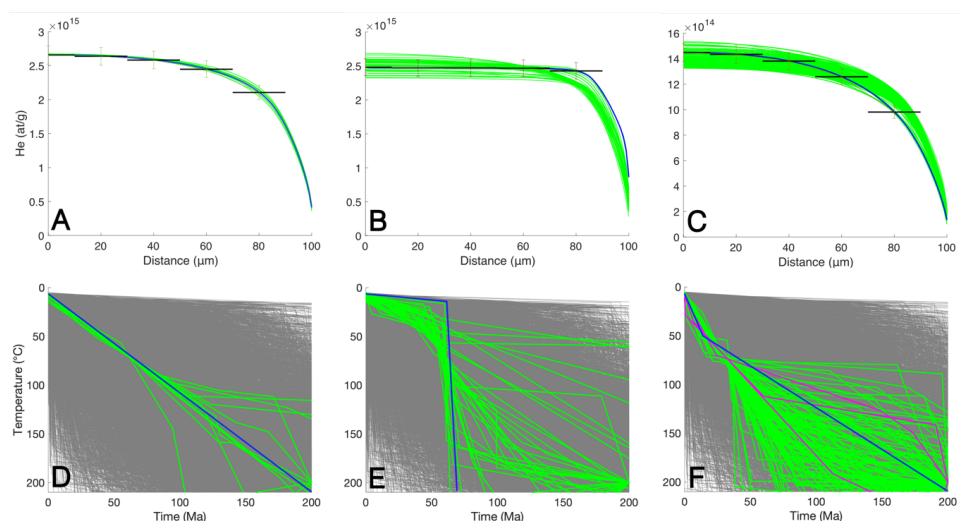


610 Fig. 10: Modelling of cooling histories for three synthetic datasets with two laser-
ablation spot measurements in apatite grains with a radius of 80 and 40 μm and U, Th, and
Sm concentrations of 10 ppm. Input cooling paths of synthetic data are shown as black lines.
A) Data was calculated with a constant cooling rate of 1°C/Myr. B) Input data were modelled
with rapid cooling at 60 Ma to surface temperature. C) Initial slow cooling with 1°C/Myr to
50°C at 10 Ma is followed by faster cooling to the surface with 4°C/Myr. Predicted cooling
615 histories with acceptable paths are green (GOF>0.05), good paths are magenta (GOF>0.5),
and paths with a GOF<0.05 are grey.

620 Second, a set of synthetically generated He measurements were taken along a profile
in a single grain. We use a cylindrical grain with a radius of 100 μm radius and the same
thermal histories as in the previous experiment. We sampled the He profile with an assumed
cylindrical spot with a diameter of 20 μm and depth of 2 μm depth at five locations from the
centre of the grain to the rim. The resulting He profiles and synthetic He measurements
(without uncertainty) along the profile are shown in Fig. 11A-C. We account for
625 measurement uncertainties by randomly sampling from a normal distribution with a mean
value corresponding to the synthetic He measurement and an assumed standard deviation
of 5%. Most acceptable cooling histories overlap or are close to the input parameters,



suggesting that in-situ (U-Th-Sm)/He measurements within a single grain can be used to get information on its cooling history.



630

Fig. 11: Cooling histories predicted from in-situ (U-Th-Sm)/He measurements sampled along the He profile of a synthetic cylindrical apatite grain with a radius of 100 μm , and U, Th, and Sm concentrations of 10 ppm. Five 20 μm diameter ablation pits across the grain (horizontal black lines) are used as synthetic input data. A-C) Synthetic He profile and input data for (i) a constant 1°C/Myr cooling rate, (ii) a rapid cooling event at 60 Ma to surface temperature, and (iii) slow cooling with 1°C/Myr to 50°C followed by faster cooling to the surface with 4°C/Myr from 10 Ma. D-F) Predicted cooling histories with acceptable paths in green (GOF > 0.05), good paths in magenta (GOF > 0.5), and paths with a GOF < 0.05 in grey. Input cooling paths of synthetic data are shown as blue lines.

640

4.0 Discussion

645

4.1 Synthesis of results

The previous results suggest that in-situ (U-Th-Sm)/He dating can provide an improvement in date and thermal history calculation compared to the conventional whole-grain analyses. This is due to the technique's capability to detect and account for radionuclide zoning, thereby resulting in reliable date predictions and thermal history

650



reconstructions. The caveat of this approach is that individual spot dates will be variable across the grain, and a framework is required for interpreting them.

Based on the previous analysis, we suggest two different measurement approaches for in-situ (U-Th-Sm)/He dates to yield geologically relevant data. These approaches include
655 single-spot measurements from multiple grains from a single sample and multiple spot locations across a single grain. In both cases, the resulting dates can be used to reconstruct the sample's cooling history for cooling rates between 1-40 °C/Myr. Faster cooling rates (e.g., 100 °C/Myr) characteristic of rapidly exhuming orogens (e.g., Himalaya, Taiwan, New Zealand) were not explored in this study and may present additional challenges if parent
660 radionuclide concentrations are low (e.g., 1-10 ppm) lending to low He concentrations that are below the detection limit.

Results presented here were based on simulated ablation pit diameters of 20 µm (2 µm deep) and U, Th, and Sm concentrations of 10 ppm. With these values, in-situ dating of apatite grains as young as ~60 Ma is possible (with our measurement limit of detection being
665 0.000079 ncc He). Accordingly, ages as young as 10 Ma can be measured with a pit diameter of 30 µm (10 µm deep). Increasing the pit volume further would be problematic for deriving the cooling history from in-situ (U-Th-Sm)/He data, especially if grains are small. Larger pit volumes integrate more likely areas of the grain affected by He ejection and limit the number of pits placed in a single grain. Given these factors, we recommend that future
670 investigations of in-situ analytical procedures analyse large grains and measure He in as small as detectable pit volumes for reconstructing thermal histories.

4.2 Meaning of in-situ dates

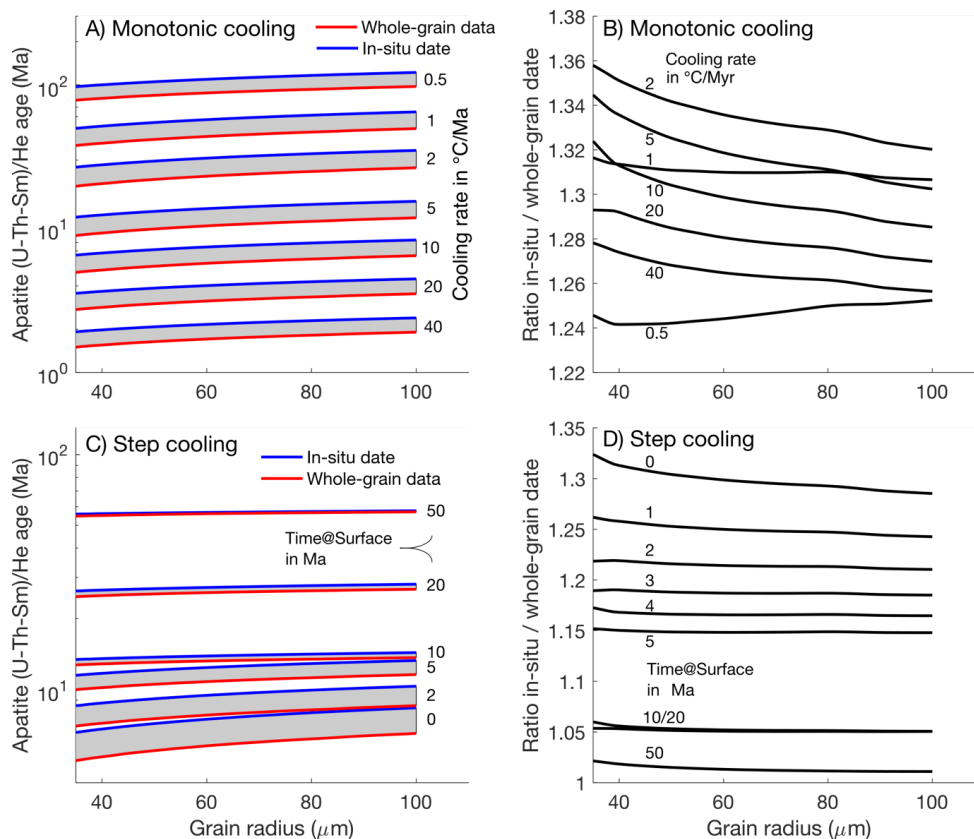
Whole-grain (U-Th-Sm)/He dates primarily depend on the cooling history and, to a lesser degree, vary with grain size, and radionuclide concentration and can occasionally be biased by radionuclide zoning or inclusions (e.g., Farley, 2002). In the rare case of quick cooling to surface temperatures, the whole-grain date (irrespective of grain size and radionuclide concentration) reflects the time of that cooling event (e.g., Wolf et al., 1998).
675 Importantly, the same date can be reproduced by slow monotonic cooling and even cooling followed by reheating (e.g. Wolf et al., 1998). In the latter case, the (U-Th-Sm)/He date might even correspond to the time when the sample was at surface temperature. A single whole-grain (U-Th-Sm)/He date alone does not hold much information on the thermal history, which requires analysis of more grains or a joint interpretation with other methods and geological
680 constraints.

Modelling in-situ and whole-grain (U-Th-Sm)/He dates for slow to fast cooling rates (1-40°C/Ma) demonstrates that dates are commonly older than the corresponding whole-grain



date for monotonic cooling (Fig. 7). In a study with a larger variation in parameters, we explored the relationship between whole-grain and in-situ dates for very slow to fast cooling rates (0.5-40°C/Ma) in more detail (Fig. 12). Monotonic cooling, irrespective of the rate, results in roughly 30% older in-situ dates compared to whole-grain dates (Fig. 12A,B). Cooling with a rate of 10°C/Myr to a surface temperature of 10°C at different times results in variable differences in whole-grain vs. in-situ dates (Fig. 12C-D). Dates are nearly identical for cooling to surface temperature at 50 Ma, and dates diverge for cooling histories to surface temperatures at younger times.

The differences in dates between the in-situ and whole-grain methods strongly depends on the cooling history and associated diffusion history. He production and ejection result in strong concentration differences in grains, which set the pace for diffusional He loss increasing from the centre to the rim of a grain, as illustrated with modelled He profiles (e.g. Fig. 11). Measuring He in the centre of grains, as is common practice in in-situ dating, leads to older ages than whole-grain dating. The latter includes diffusion-related He-depleted grain rims, yielding younger dates. Samples where the majority of produced He has not been affected by high diffusion rates have similar whole-grain and in-situ dates, such as in the rapidly cooled Fish Canyon age standard (e.g. Horne et al., 2016; Pickering et al., 2020) or Ellendale pipe samples (Evans et al., 2015). In one additional scenario, whole-grain and in-situ dates are anticipated to exhibit identical dates. This occurs with super-large crystals irrespective of their specific cooling history, exemplified by Durango apatite and Madagascar monazite and zircon (see Boyce et al., 2006; Evans et al., 2015; Horne et al., 2018; Vermeesch et al., 2012).



710

Fig. 12: Whole-grain vs. in-situ (U-Th-Sm)/He dates as a function of grain size and cooling rate for a U, Th, and Sm concentration of 10 ppm (homogenously distributed) and assuming a single spot radius of 10 μm (2 μm deep) in the centre of a spherical grain. A) Dates for cooling rates of 0.5 to 40 $^{\circ}\text{C}/\text{Myr}$. B) Ratio of in-situ and whole-grain dates as a function of grain size and cooling rate. C-D) Same as A and B, but modelled with a step cooling to surface temperature (10 $^{\circ}\text{C}$) at different times (0-50 Ma) with a cooling rate of 10 $^{\circ}\text{C}/\text{Myr}$.

720

The fundamental difference between whole-grain and in-situ (U-Th-Sm)/He dating is the location and volume where He is measured in a grain. The simulations presented here reveal that the resulting in-situ dates, except for gemstones and age standards, will be significantly older (~30% for monotonic cooling) than whole-grain dates. Previous studies mainly focused on age standards and gemstones for which in-situ and whole-grain dates can be expected to be similar (e.g. Boyce et al., 2006; Evans et al., 2015; Horne et al., 2018; Vermeesch et al., 2012). Our simulations revealed that applying in-situ dating to samples

725



other than age standards or super-large gemstone crystals and comparing it to available whole-grain dates requires thermal history modelling to calculate corresponding whole-grain dates.

730 Tipathy-Lang et al. (2013) analysed detrital zircons from a tributary of the Indus River in the Himalayas, draining the southern part of the Ladakh batholith, with the in-situ method. Cooling of the Ladakh batholith through the partial retention zone of He in zircons likely occurred rapidly in Oligocene times (Kirstein et al., 2009). According to our modelling results, this should result in similar whole-grain and in-situ zircon dates. In fact, the resulting whole-grain and in-situ date distributions show comparable patterns, with slightly older whole-grain dates (mean date 29 vs. 26 Ma). Tipathy-Lang et al. (2013) interpreted the difference to result from preferential grain selection for whole-grain analyses and considered the in-situ dates to be more representative. Alternatively, the larger spread and slight shift to older dates may be based on methodological differences, where in-situ dates are generally older
740 for samples that have experienced diffusional He loss.

In summary, in-situ (U-Th-Sm)/He dating of apatite/zircon is an alternative to whole-grain dating with obvious advantages. However, our modelling results demonstrate that dates cannot simply be interpreted together with whole-grain data. If analysed grains are expected to have lost a significant fraction of He by diffusion, in-situ dates will be older than
745 whole-grain dates. In the case of bedrock studies, in-situ data can be interpreted using modified thermal models introduced here, and to aid comparisons to existing whole-grain datasets, corresponding whole-grain data can be derived from those models. In most detrital studies, it is impossible to know the fractional loss of He of each individual grain and in-situ dates, if measured in the centre of grains, will be systematically older. In case the dates of
750 source areas are largely different (e.g., 15 vs. 30 vs. 90 Ma), inferences from in-situ (U-Th-Sm)/He dating might still be acceptable, such as the detrital zircon study from the Inn River in the European Alps by Dunkl et al. (2024).

755 4.3 Grain selection considerations for in-situ measurement

Grain selection for the in-situ (U-Th-Sm)/He method follows criteria similar to the whole-grain method. Simple 1D thermal history modelling requires that selected grains have smooth surfaces and are symmetrical, such as spheres and cylinders. The long-prismatic
760 shape and basal cleavage direction often result in the fragmentation of apatite grains, especially during the mineral separation process (e.g., Farley, 2002). Interpreting apatite fragments with the whole-grain and $^4\text{He}/^3\text{He}$ method usually requires corrections for grain fragmentation (e.g., Brown et al., 2013; Flowers and Farley, 2012). Instead, fragments of



apatite grains broken along the basal faces can be treated similarly to intact grains with the
765 in-situ (U-Th-Sm)/He method.

Grains should be free of inclusions to avoid excess He from long-alpha stopping
distances (e.g., Farley, 2002). The pre-measurement exposure of the inner surface
facilitates thorough inspection of the grain interior and identification of potential inclusions at
770 sub- μm resolution using 1000x magnification. Even though not visually evident with
microscopy, inclusions can be identified by measuring radionuclide concentrations with LA-
ICP-MS. The downside of analyzing inner surfaces after abrasion is that roughly half of the
grain is not available for inspection, and thus outliers related to excess He from mineral
inclusions (abraded away) will still be an issue in in-situ (U-Th-Sm)/He dating.

Similar to the whole-grain method, reliable date determination and thermal history
775 reconstructions require precise measurements of grain geometries (e.g., Glotzbach et al.,
2019). Future applications of the in-situ (U-Th-Sm)/He methodology will show if geometry
measurements are required before embedding grains, or measurements can be done within
the mount following grain selection. Measurements of the distance between He laser pits
and grain prism faces can follow pit volume measurements. An issue that may arise is the
780 complexity involved in accurately determining the position of the inner surface relative to the
original grain boundary, particularly in the vertical orientation. The common tetragonal and
hexagonal cross-sectional shapes of zircons and apatites result in theoretically variable-
sized inner surfaces (e.g. Fig. 6). A symmetrical apatite and simple zircon grain have a ratio
between circum- to inner radius of 1/1.15 and 1/1.41, respectively. It is, therefore, mandatory
785 to accurately determine the correct location of the pit location with respect to the whole grain
geometry.

4.4 Recommended reporting procedure for in-situ analytical data.

790 Based on the model results presented here and the discussion in the previous section,
we recommend reporting of several different aspects of in-situ measurements. These items
will enable not only reproduction of dates for each spot, but also facilitate modeling of grain
thermal histories using the software of this study. Essential items to report in data tables for
each grain include: 1) grain geometry (preferably with photos in a supplement) and assumed
795 grain geometry (e.g., sphere, infinite cylinder, other) used for age calculation, 2) (for each
ablation pit across a grain) the pit diameter, measured volume, depth, and center point of the
pit relative to the a-, b- and c-axis of the grain, 3) the He measured from the ablation bit, 4)
the U, Th and Sm concentration profiles, 5) the calculated in-situ grain date, and 6) the
whole-grain equivalent date (does require thermal history modelling, see Fig. 12). Reporting
800 of the above information enables thermal history modeling of individual grains and



comparison of in-situ dates to whole-grain dates from neighbouring areas and/or previous studies.

4.5 Future considerations

805

Although the theoretical benefits and limitations have been explored here, more applications of the in-situ (U-Th-Sm)/He method to regular samples are required. Future studies should explore (i) the spatial relationship between radionuclide zoning and resulting He distribution, and (ii) the reliability of in-situ (U-Th-Sm)/He-derived thermal history reconstructions. Lastly (iii), as previously mentioned, future modelling studies should evaluate tradeoffs between the cooling rate (particularly at higher cooling rates of >10 °C/Myr) and parent radionuclide concentrations to evaluate the limits of in-situ dating to produce geologically interpretable data.

815

5.0 Conclusions

This study examined the theoretical relationship between the parent radionuclide distribution and the resulting He concentrations within a grain (such as apatite or zircon). This was done using an updated version of the production, ejection, and diffusion model (i.e., RDAAM). We investigated the dependencies of predicted whole-grain and in-situ apatite and zircon (U-Th-Sm)/He dates for monotonic cooling histories (1-40 °C/Myr), grain size (40-100 μm), and (in the case of in-situ data) the position of the measurement within the grain. In addition, we explored strategies for reconstructing the thermal history from multiple and single apatite grains.

Model predictions revealed that the He concentration and resulting in-situ date is mainly a function of the grain size, eU, and distance to the grain rim. Thus, the interpretation of in-situ (U-Th-Sm)/He dates necessitates the assessment of the grain geometry of the measured grains and determining the distance between the laser spot and the closest prismatic face. Most importantly, in-situ dates for samples that experienced diffusional He loss will be older than whole-grain dates. In most cases, understanding in-situ data necessitates the application of adapted thermal models introduced in this study. Additionally, to facilitate comparison with existing whole-grain data, corresponding whole-grain dates can be determined through thermal history modelling.

Our observations revealed that radionuclide zoning is not an anomaly but a prevalent occurrence in both apatite and zircon. Analysis of a substantial dataset using LA-ICP-MS for radionuclide measurements in these minerals demonstrated that the observed radionuclide



840 zoning has, if disregarded, the potential to substantially skew the relationships between
effective uranium (eU) and whole-grain dates. Furthermore, results suggest that a minimum
of 10 apatite grains are needed to reach an R^2 of 0.8 between eU and date and a labour-
intensive number (23) of whole-grain ZHe dates is needed to reach a minimum R^2 of 0.5
between eU and date.

845 Two promising approaches exist for reconstructing the thermal history of rocks using
the in-situ (U-Th-Sm)/He method. Similar to data obtained from whole grains, variations in
grain size and/or effective uranium content, which lead to differences in helium diffusivity and
in-situ dates, can be utilized for thermal history reconstructions. The in-situ (U-Th-Sm)/He
method can measure a He concentration profile in single grains, which is, among other
factors, controlled by the cooling history. Modelling results suggest that several in-situ (U-Th-
Sm)/He measurements along a profile from the centre of a grain to the prism face can be
850 inverted to reconstruct the thermal history of a single grain.

Author contribution

Conceptualization: CG, TE

Formal analysis: CG

855 Investigation: CG

Methodology: CG

Software: CG

Visualization: CG

Writing: CG, TE

860

Competing interests

The contact author has declared that none of the authors has any competing interests.

Acknowledgements

865 This study was supported by (1) the Deutsche Forschungsgemeinschaft (DFG) to
Christoph Glotzbach (GL 724/11-1) under the priority program 4D-MB and is a contribution
to the AlpArray initiative, (2) the Bundesgesellschaft für Endlagerung (BGE – STAFuE-21-
12-Klei), and (3) a large equipment funding by the DFG to Todd Ehlers (INST 37/1041-1
FUGG). The manuscript benefitted from discussions with Sarah Falkowski and Ann-Kathrin
870 Maier.

6.0 References Cited



- Anderson, A. J., Hodges, K. V., and van Soest, M. C.: Empirical constraints on the effects of
875 radiation damage on helium diffusion in zircon, *Geochimica et Cosmochimica Acta*,
218, 308–322, <https://doi.org/10.1016/j.gca.2017.09.006>, 2017.
- Bragg, W. H., and Kleeman, R.: On the α particles of radium, and their loss of range in
passing through various atoms and molecules. *The London, Edinburgh, and Dublin
Philosophical Magazine and Journal of Science*, 10(57), 318–340,
880 <https://doi.org/10.1080/14786440509463378>, 1905.
- Ehlers, T. A.: Crustal Thermal Processes and the Interpretation of Thermochronometer Data,
Reviews in Mineralogy and Geochemistry, 58(1), 315–350,
<https://doi.org/10.2138/rmg.2005.58.12>, 2005.
- Ehlers, T. A. and Farley, K. A.: Apatite (U–Th)/He thermochronometry: methods and
885 applications to problems in tectonic and surface processes, *Earth and Planetary
Science Letters*, 206, 1–14, [https://doi.org/10.1016/S0012-821X\(02\)01069-5](https://doi.org/10.1016/S0012-821X(02)01069-5), 2003.
- Danišík, M., McInnes, B. I. A., Kirkland, C. L., McDonald, B. J., Evans, N. J., and Becker, T.:
Seeing is believing: Visualization of He distribution in zircon and implications for
thermal history reconstruction on single crystals, *Science Advances*, 3(2), e1601121,
890 <https://doi.org/10.1126/sciadv.1601121>, 2017.
- Falkowski, S., Ehlers, T. A., McQuarrie, N., Glover, C. O., Perez, N. D., and Buford Parks, V.
M.: Exhumation and incision of the eastern Central Andes, southern Peru: Low-
temperature thermochronology observations, *Earth and Planetary Science Letters*,
620, 118299, <https://doi.org/10.1016/j.epsl.2023.118299>, 2023.
- 895 Farley, K. A., Wolf, R. A., and Silver, L. T.: The effects of long alpha-stopping distances on
(U–Th–Sm)/He dates, *Geochimica et Cosmochimica Acta*, 60(21), 4223–4229,
[https://doi.org/10.1016/s0016-7037\(96\)00193-7](https://doi.org/10.1016/s0016-7037(96)00193-7), 1996.
- Farley, K. A.: Helium diffusion from apatite: General behavior as illustrated by Durango
fluorapatite, *Journal of Geophysical Research: Solid Earth*, 105(B2), 2903–2914,
900 <https://doi.org/10.1029/1999JB900348>, 2000.
- Farley, K. A.: (U–Th–Sm)/He Dating: Techniques, Calibrations, and Applications, *Reviews in
Mineralogy and Geochemistry*, 47(1), 819–844,
<https://doi.org/10.2138/rmg.2002.47.18>, 2002.
- Farley, K. A., Shuster, D. L., Watson, E. B., Wanser, K. H., and Balco, G.: Numerical
905 investigations of apatite $^4\text{He}/^3\text{He}$ thermochronometry: APATITE $^4\text{He}/^3\text{He}$
THERMOCHRONOMETRY, *Geochemistry, Geophysics, Geosystems*, 11(10),
<https://doi.org/10.1029/2010GC003243>, 2010.
- Farley, K. A., Shuster, D. L., and Ketcham, R. A.: U and Th zonation in apatite observed by
laser ablation ICPMS, and implications for the (U–Th)/He system, *Geochimica et*



- 910 Cosmochimica Acta, 75(16), 4515–4530, <https://doi.org/10.1016/j.gca.2011.05.020>, 2011.
- Flowers, R. M.: Exploiting radiation damage control on apatite (U–Th)/He dates in cratonic regions, *Earth and Planetary Science Letters*, 277(1–2), 148–155, <https://doi.org/10.1016/j.epsl.2008.10.005>, 2009.
- 915 Flowers, R. M., Ketcham, R. A., Shuster, D. L., and Farley, K. A.: Apatite (U–Th)/He thermochronometry using a radiation damage accumulation and annealing model, *Geochimica et Cosmochimica Acta*, 73(8), 2347–2365, <https://doi.org/10.1016/j.gca.2009.01.015>, 2009.
- Fox, M., McKeon, R. E., and Shuster, D. L.: Incorporating 3-D parent nuclide zonation for apatite $^4\text{He}/^3\text{He}$ thermochronometry: An example from the Appalachian Mountains, *Geochemistry, Geophysics, Geosystems*, 15(11), 4217–4229, <https://doi.org/10.1002/2014GC005464>, 2014.
- 920 Gallagher, K., Brown, R., and Johnson, C.: Fission track analysis and its applications to geological problems, *Annual Review of Earth and Planetary Sciences*, 26(1), 519–572, <https://doi.org/10.1146/annurev.earth.26.1.519>, 1998.
- Gautheron, C., Tassan-Got, L., Barbarand, J., and Pagel, M.: Effect of alpha-damage annealing on apatite (U–Th)/He thermochronology, *Chemical Geology*, 266(3–4), 157–170, <https://doi.org/10.1016/j.chemgeo.2009.06.001>, 2009.
- 930 Glotzbach, C., Lang, K. A., Avdievitch, N. N., and Ehlers, T. A.: Increasing the accuracy of (U–Th–Sm)/He dating with 3D grain modelling, *Chemical Geology*, 506, 113–125, <https://doi.org/10.1016/j.chemgeo.2018.12.032>, 2019.
- Guenther, W. R., Reiners, P. W., Ketcham, R. A., Nasdala, L., and Giester, G.: Helium diffusion in natural zircon: Radiation damage, anisotropy, and the interpretation of zircon (U–Th–Sm)/He thermochronology, *American Journal of Science*, 313(3), 145–198, <https://doi.org/10.2475/03.2013.01>, 2013.
- 935 Guenther, W. R., Reiners, P. W., Drake, H., and Tillberg, M.: Zircon, titanite, and apatite (U–Th–Sm)/He dates and date–eU correlations from the Fennoscandian Shield, southern Sweden: Fennoscandian Zirc He Date–eU Correlation, *Tectonics*, 36(7), 1254–1274, <https://doi.org/10.1002/2017TC004525>, 2017.
- 940 House, M. A., Farley, K. A., and Stockli, D.: Helium chronometry of apatite and titanite using Nd–YAG laser heating, *Earth and Planetary Science Letters*, 183(3–4), 365–368, [https://doi.org/10.1016/S0012-821X\(00\)00286-7](https://doi.org/10.1016/S0012-821X(00)00286-7), 2000.
- 945 Horne, A. M., van Soest, M. C., Hodges, K. V., Tripathy–Lang, A., and Hourigan, J. K.: Integrated single crystal laser ablation U/Pb and (U–Th)/He dating of detrital accessory minerals – Proof-of-concept studies of titanites and zircons from the Fish Canyon tuff,



- Geochimica et Cosmochimica Acta, 178, 106–123,
<https://doi.org/10.1016/j.gca.2015.11.044>, 2016.
- 950 Horne, A. M., van Soest, M. C., and Hodges, K. V.: U/Pb and (U-Th-Sm)/He “double” dating
of detrital apatite by laser ablation: A critical evaluation, *Chemical Geology*, 506, 40–
50, <https://doi.org/10.1016/j.chemgeo.2018.12.004>, 2019.
- Hourigan, J. K., Reiners, P. W., and Brandon, M. T.: U-Th zonation-dependent alpha-
ejection in (U-Th)/He chronometry, *Geochimica et Cosmochimica Acta*, 69, 3349–
3365, <https://doi.org/10.1016/j.gca.2005.01.024>, 2005.
- 955 Ketchum, R. A.: Forward and Inverse Modeling of Low-Temperature Thermochronometry
Data. *Reviews in Mineralogy and Geochemistry*, 58(1), 275–314,
<https://doi.org/10.2138/rmg.2005.58.11>, 2005.
- Kirstein, L. A., Foeken, J. P. T., van der Beek, P., Stuart, F. M., and Phillips, R. J.: Cenozoic
unroofing history of the Ladakh Batholith, western Himalaya, constrained by
thermochronology and numerical modelling, *Journal of the Geological Society*, 166,
960 667–678, <https://doi.org/10.1144/0016-76492008-107>, 2009.
- Lippolt, H. J., Leitz, M., Wernicke, R. S., and Hagedorn, B.: (Uranium + thorium)/helium
dating of apatite: experience with samples from different geochemical environments,
Chemical Geology, 112(1–2), 179–191, [https://doi.org/10.1016/0009-2541\(94\)90113-9](https://doi.org/10.1016/0009-2541(94)90113-9), 1994.
- 965 Malusà, M. G., and Fitzgerald, P. G. (Ed.): *Fission-track thermochronology and its
application to geology*. Springer, 393 p, <https://doi.org/10.1007/978-3-319-89421-8>,
2019.
- McDowell, F. W., McIntosh, W. C., and Farley, K. A.: A precise ^{40}Ar – ^{39}Ar reference date for
the Durango apatite (U–Th)/He and fission-track dating standard, *Chemical Geology*,
970 214(3–4), 249–263, <https://doi.org/10.1016/j.chemgeo.2004.10.002>, 2005.
- Meesters, A. G. C. A., and Dunai, T. J.: Solving the production–diffusion equation for finite
diffusion domains of various shapes, *Chemical Geology*, 186(3–4), 333–344,
[https://doi.org/10.1016/S0009-2541\(01\)00422-3](https://doi.org/10.1016/S0009-2541(01)00422-3), 2002.
- 975 Pickering, J., Matthews, W., Enkelmann, E., Guest, B., Sykes, C., and Koblinger, B. M.:
Laser ablation (U-Th-Sm)/He dating of detrital apatite, *Chemical Geology*, 548,
119683, <https://doi.org/10.1016/j.chemgeo.2020.119683>, 2020.
- Reiners, P. W.: Zircon (U-Th-Sm)/He Thermochronometry, *Reviews in Mineralogy and
Geochemistry*, 58(1), 151–179, <https://doi.org/10.2138/rmg.2005.58.6>, 2005.
- 980 Reiners, P. W. and Ehlers, T. A.: Low-temperature thermochronology: Techniques,
interpretations and applications, *Reviews in Mineralogy and Geochemistry*, 58(1),
<https://doi.org/10.2138/rmg.2005.58.0>, 2005.



- Reiners, P. W., and Brandon, M. T.: Using thermochronology to understand orogenic erosion, *Annu. Rev. Earth Planet. Sci.*, 34, 419–466, <https://doi.org/10.1146/annurev.earth.34.031405.125202>, 2006.
- 985 Shuster, D. L., and Farley, K. A.: $4\text{He}/3\text{He}$ thermochronometry, *Earth and Planetary Science Letters*, 217(1–2), 1–17, [https://doi.org/10.1016/S0012-821X\(03\)00595-8](https://doi.org/10.1016/S0012-821X(03)00595-8), 2004.
- Spiegel, C., Kohn, B., Belton, D., Berner, Z., and Gleadow, A.: Apatite (U–Th–Sm)/He thermochronology of rapidly cooled samples: The effect of He implantation, *Earth and Planetary Science Letters*, 285(1–2), 105–114, <https://doi.org/10.1016/j.epsl.2009.05.045>, 2009.
- 990 Vermeesch, P., Seward, D., Latkoczy, C., Wipf, M., Günther, D., and Baur, H.: α -Emitting mineral inclusions in apatite, their effect on (U–Th)/He dates, and how to reduce it, *Geochimica et Cosmochimica Acta*, 71(7), 1737–1746, <https://doi.org/10.1016/j.gca.2006.09.020>, 2007.
- 995 Wolf, R. A., Farley, K. A., and Silver, L. T.: Helium diffusion and low-temperature thermochronometry of apatite, *Geochimica et Cosmochimica Acta*, 60(21), 4231–4240, [https://doi.org/10.1016/s0016-7037\(96\)00192-5](https://doi.org/10.1016/s0016-7037(96)00192-5), 1996.